Acta Astronautica 186 (2021) 473–485

Contents lists available at ScienceDirect

Acta Astronautica

journal homepage: www.elsevier.com/locate/actaastro

Research paper

# Precise power descent control of a lunar lander using a single thruster

Rolando Cortés-Martínez [a,1], Krishna D. Kumar [a,*,2], H. Rodríguez-Cortés [b,3]

[a] Department of Aerospace Engineering, Ryerson University, Toronto, Ontario M5B 2K3, Canada
[b] Departamento de Ingeniería Eléctrica, Centro de Investigación y de Estudios Avanzados del Instituto Politécnico Nacional, Mexico

## ABSTRACT

This paper addresses the problem of powered descent control of a lunar lander during its final landing phase, where soft and precise landing at the target cite is required. In the literature, this problem has been solved considering a fully actuated lunar lander. Recently, landers are designed as complex systems with several onboard payloads and subsystems for completing demanding mission tasks. There are increasing constraints on mass budget and space availability onboard a lander. In order to meet these requirements, a novel controller using a single thruster is proposed. The proposed controller has three control inputs (thrust and two gimbaled angles) to control the six degrees of motion of a lander; these control inputs are non-affine. The proposed controller is designed based on variable structure control technique augmented with a high order filter, an immersion and invariance-based mass estimator and a sliding mode angular velocity observer. The stability analysis using Lyapunov theory and the results of the numerical simulations along with Monte Carlo simulations of the system show that the precise landing of the lunar lander using a single thruster is feasible.

## 1. Introduction

In recent years, the interest in exploration missions to the Moon has arisen. The most recent mission, the lander Chang'e 4 [1], represents one of many other landing missions that might take place in the following years. From the different phases that make up the powered descending, the final stage close to the touchdown requires a soft and precise landing at the target site. This paper focuses on the final stage. Most of the moon landing missions made so far are characterized by having independent groups of actuators for attitude control and descent trajectory tracking control. This fully actuated lunar lander missions require one main thruster to control the descent maneuver and a reaction control system (RCS) comprised of pairs of smaller jets or thrusters to command the attitude control. The recent missions Chang'e 3 and Chang'e 4 [1] employed a set of up to 29 thrusters (one main engine with an adjustable throttle for powered descending, and the rest for attitude control). A Proportional Integral Control (PID) scheme solves the attitude and position regulation problems. Other control laws, for fully actuated lunar landers, are reported in [2] and [3]. The work in [2] presented a controller based on a virtual trajectory represented by dual quaternions. The results show pinpoint, soft-landing, and robustness against noise in measurements. Moreover, the lunar lander uses the main thruster to control its descent while a group of reaction thrusters is provided to control its attitude. The same actuation configuration is assumed in [3], wherein an integrated control law is derived, which considers the translational dynamics and the rotational dynamics as a coupled system, providing a solution to the final descent stage.

Thrust Vector Control (TVC), is another option for spacecraft control. TVC is a general term referred to a control system designed to tilt the direction of the thrust vector with respect to the spacecraft body frame. There are different approaches to achieve TVC, like reactive fluid injection, vanes, auxiliary engines, and gimbaled engines. Some aircraft/rockets have used TVC to control their attitude in different landing applications as reported in [4,5] and [6]. The TVC has also been used in the descending engine of the Apollo mission [7], where a gimbaled thruster aligns the thrust vector through the center of mass (CM), with speed constrained actuators. A third-order control algorithm computes the time that every actuator to be turned on to attain the desired attitude in minimum time. The control design does not consider coupling effects of force and torque of the actuator, and it solves the attitude control problem only. Another limitation is that the gimbal angles are actuated at a preset constant angular rate of $\pm 0.2$ rad/s. In [8], a lunar lander physical simulator is considered along with a gimbaled thruster and a group of reaction thrusters providing torque only around the vertical axis. A simple guidance strategy is tested solving the regulation problem for different altitude commands.

Some works have used gimbal thrusters for spacecraft attitude control. In [9], a control algorithm using a single thruster is designed to deal with disturbances and parametric uncertainties. To address the non-affine control inputs problem (nonlinear control inputs), a filter

* Corresponding author.
*E-mail address:* kdkumar@ryerson.ca (K.D. Kumar).
[1] Ph.D. visiting student, Ryerson University, Department of Aerospace Engineering, Ryerson University, Toronto, Ontario, ON M5B 2K3, Canada.
[2] Professor, Department of Aerospace Engineering, Ryerson University, Toronto, Ontario, ON M5B 2K3, Canada, Associate Fellow and Life Member of AIAA.
[3] Professor, Department of Electrical Engineering, Centro de Investigación y de Estudios Avanzados del Instituto Politécnico Nacional, Mexico City, Mexico.

https://doi.org/10.1016/j.actaastro.2021.06.001
Received 7 January 2021; Received in revised form 11 April 2021; Accepted 1 June 2021
Available online 6 June 2021

**Nomenclature**

| | |
|---|---|
| $0_{i\times j}$ | Zero elements matrix ($i \times j$) |
| $\boldsymbol{a_c}$ | Acceleration in cylindrical coordinates ($3 \times 1$) |
| $A, B$ | Dynamic system matrices |
| $c_i$ | Column vectors ($3 \times 1$) |
| CM | Center of mass |
| $D$ | Terminal time for landing, s |
| $\boldsymbol{F_a}$ | Thrust of actuator ($3 \times 1$), N |
| $F$ | Norm of thrust of actuator, N |
| $\boldsymbol{F_g}$ | Gravity force vector ($3 \times 1$), N |
| $I_3$ | Identity matrix ($3 \times 3$) |
| $J$ | Moment of inertia matrix ($3 \times 3$), kg m$^2$. |
| $J_R$ | Actuator Jacobian matrix for rotational dynamics |
| $J_T$ | Actuator Jacobian matrix for translational dynamics |
| $k_m, k_{m2}, k_\beta, k_o$ | Positive constants |
| $K_a$ | $diag(k_1, k_2, k_3)$ matrix gain ($3 \times 3$) |
| $K_{lqr}$ | Matrix gain ($3 \times 7$) |
| $l$ | Distance between gimbal pivot and CM |
| $m$ | Mass, kg |
| $m_i$ | Inverse of mass, 1/kg |
| $\boldsymbol{p}$ | Position in cylindrical coordinates ($3 \times 1$) |
| $R$ | Rotation matrix from local frame to body frame |
| $r_m$ | Radius of the moon, m |
| $S$ | Sliding surface |
| $S_z$ | Sliding surface in terms of Z |
| $T$ | Transformation matrix |
| $U$ | $[F, \beta_1, \beta_2]^\top$ control input vector |
| $U_d$ | Time derivative of $U$ |
| $\boldsymbol{v_c}$ | Velocity in cylindrical coordinates ($3 \times 1$) |
| $W$ | Rotational kinematics matrix |
| $x, r, \theta$ | Cylindrical coordinates components, m, m, rad |
| $X$ | State vector ($12 \times 1$) |
| $Z$ | State vector transformed by T |
| $\alpha_o$ | Velocity observer gain |
| $\beta_1$ | Deflection angle 1 of gimbal thruster, rad |
| $\beta_2$ | Deflection angle 2 of gimbal thruster, rad |
| $\chi$ | Position of gimbal pivot from CM, m |
| $\delta_o$ | Velocity observer parameter |
| $\lambda_o$ | Velocity observer gain |
| $\Lambda_i$ | Elements of rotation matrix around $\alpha$ |
| $\Gamma$ | Matrix for sliding surface definition ($3 \times 12$) |
| $\mu$ | Moon gravitational parameter, m$^3$/s$^2$ |
| $\Omega$ | Lander angular rates ($3 \times 1$), rad/s. |
| $\omega_i$ | ith-component of angular momentum, kg m$^2$/sec |
| $\boldsymbol{\Phi}$ | $[\alpha\ \phi\ \gamma]^\top$, Euler angles, rad. |
| $\psi$ | Control robust term ($3 \times 1$) |
| $\sigma$ | High order sliding surface ($3 \times 1$) |
| $\boldsymbol{\tau_a}$ | Torque produce by actuator ($3 \times 1$), N m |
| $\boldsymbol{\tau_g}$ | Torque produce by disturbances ($3 \times 1$), N m |
| $\xi$ | Generic state variable |
| $\zeta_{o1}, \zeta_{o2}$ | Velocity observer correction variables |

**Subscripts**

| | |
|---|---|
| $a$ | Actuator |
| $b$ | Body frame |
| $c$ | Controllable |
| $d$ | Desired |
| $i$ | Inertial frame |
| $L$ | Linear |
| $r$ | Reference |
| $t$ | Target |
| $x, y, z$ | Cartesian components |
| $uc$ | Uncontrollable |

that allows extracting uncoupled time derivatives of the thruster gimbal angle inputs is proposed. The equations of motion consider that the spacecraft is in an orbit, which allows reducing some nonlinear terms. In [10], there is a study of different configurations of two or more gimbal thrusters to carry out attitude control. Some works consider control of underactuated spacecraft. In [11] it is considered the attitude control problem of underactuated spacecraft in orbit. In [12] a formation flying orbiting Earth is studied; there are two underactuated cases of study, wherein radial direction or along-track direction actuation is not present.

In this paper, we consider an underactuated lunar lander, equipped with a single gimbaled thruster, to carry out a pinpoint and soft powered descend on the Moon's surface. The control inputs of the system are non-affine, which makes the controller design a challenging problem. To the best of our knowledge, the lunar lander soft landing problem in the underactuated configuration has not been studied. The major contributions of the paper are as follows:

1. A novel nonlinear controller using a single thruster onboard a lander is designed to control its motion in presence of its unknown mass and without angular velocity measurements.
2. A lander's mass observer is designed based on the Immersion and Invariance technique while the sliding mode theory is considered to design a lander's angular velocity observer.
3. The stability of the closed-loop system is proven using Lyapunov theory. Finally, the numerical simulations along with Monte Carlo simulations validate the feasibility of the proposed controller.

## 2. System model

The proposed system comprises a lunar lander with a gimbaled thruster (Fig. 1). Both the lunar lander and the thruster are assumed to be rigid bodies while the Moon is considered a point mass. The onboard thruster is used to control position as well as the attitude of the lander. The position of the lander $\boldsymbol{p} = [x\ r\ \theta\ ]^\top$ is described in cylindrical coordinates, with respect to the inertial frame $O - X_iY_iZ_i$ attached to the center of mass of the Moon (Fig. 2), $r$ is the radius of the projection of $\boldsymbol{p}$ onto the $Y_iZ_i$ plane, $\theta$ is the angle of this projection measured from the $Y_i$-axis, and $x$ is the component of $\boldsymbol{p}$ along the $X_i$-axis. The $X_i$-axis is aligned with the axis of rotation of the Moon.

The attitude of the lander is described in terms of Euler angles with respect to its body-fixed frame, $S - X_bY_bZ_b$ (Fig. 3). The 3-2-1 Euler angles sequence ($\alpha$ (roll), $\phi$ (pitch) and $\gamma$ (yaw)) is considered [13] and the corresponding rotational matrix $R$ which transforms the coordinates in the local reference frame, $O - X_LY_LZ_L$ (cylindrical frame) to the coordinates in the lander body-fixed frame, $S - X_bY_bZ_b$ (Fig. 3) is given by

$$R = R_z(\gamma)R_y(\phi)R_x(\alpha) \tag{1}$$

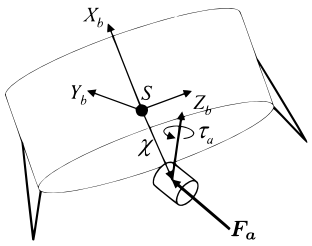


**Fig. 1.** System model: a lunar lander with a thruster.

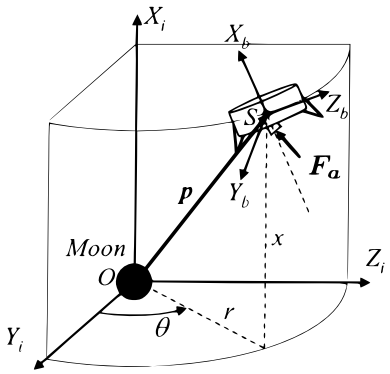


**Fig. 2.** System translational motion in cylindrical coordinates.

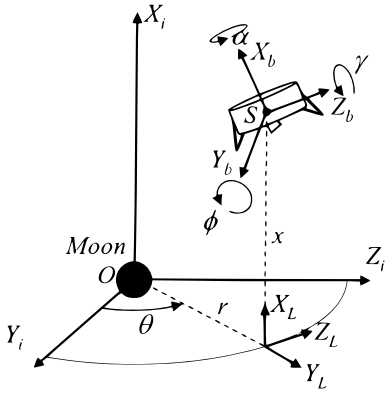


**Fig. 3.** Lunar lander attitude motion in Euler angles.

where

$$R_x(\alpha) = \begin{bmatrix} 1 & 0 & 0 \\ 0 & c_\alpha & s_\alpha \\ 0 & -s_\alpha & c_\alpha \end{bmatrix}$$

$$R_y(\phi) = \begin{bmatrix} c_\phi & 0 & -s_\phi \\ 0 & 1 & 0 \\ s_\phi & 0 & c_\phi \end{bmatrix}$$

$$R_z(\gamma) = \begin{bmatrix} c_\gamma & s_\gamma & 0 \\ -s_\gamma & c_\gamma & 0 \\ 0 & 0 & 1 \end{bmatrix}.$$

Here $c_x$ and $s_x$ stand for $\cos(x)$ and $\sin(x)$, respectively. It is to be noted that the selected 3-2-1 Euler angles sequence ($\alpha$ (roll), $\phi$ (pitch) and $\gamma$ (yaw)) has singularity only at $\phi$ (pitch) = ± 90 degrees. Thus, the singularity problem is avoided assuming $\phi$ (pitch) is below ± 90 degrees throughout the final landing phase; this assumption is consistent in relation to the practical planetary lander missions, wherein the attitude angles, especially pitch and yaw angles, of a lander are well below ± 90 degrees during the final landing phase.

The translational model of the system is obtained as

$$m\boldsymbol{a_c} = \boldsymbol{F_g} + R^\top \boldsymbol{F_a} \tag{2}$$

where $m$ is the system mass including mass of the lander and thruster, $\boldsymbol{a_c} = \frac{d^2}{dt^2}(x\hat{x} + r\hat{r})$ is the system acceleration vector given in cylindrical coordinates [14] with $\hat{x}$, $\hat{r}$ as the unit vectors along the $X_L$-axis and $Y_L$-axis, respectively (Fig. 3), $R$ is the rotational matrix (Eq. (1)), $\boldsymbol{F_g}$ is the force due to the Moon's gravity, and $\boldsymbol{F_a}$ is the control force due to the gimbaled thruster. The system mass, $m$ is assumed to be constant but unknown. The translational model of the system, given by Eq. (2), can be written in the scalar form as follows:

$$\ddot{x} = \frac{1}{m} e_1^\top \boldsymbol{F_g} + \frac{1}{m} e_1^\top R^\top \boldsymbol{F_a} \tag{3}$$

$$\ddot{r} = \frac{1}{m} e_2^\top \boldsymbol{F_g} + r\dot{\theta}^2 + \frac{1}{m} e_2^\top R^\top \boldsymbol{F_a} \tag{4}$$

$$\ddot{\theta} = \frac{-2\dot{r}\dot{\theta}}{r} + \frac{1}{mr} e_3^\top R^\top \boldsymbol{F_a} \tag{5}$$

where $e_1 = [1\ 0\ 0]^\top$, $e_2 = [0\ 1\ 0]^\top$, $e_3 = [0\ 0\ 1]^\top$. The system attitude kinematics and dynamics are described by the following set of differential equations:

*Kinematics*

$$\dot{\boldsymbol{\Phi}} + e_1\dot{\theta} = W^{-1}\Omega \tag{6}$$

*Dynamics*

$$J\dot{\Omega} = J\Omega \times \Omega + \boldsymbol{\tau_g} + \boldsymbol{\tau_a} \tag{7}$$

where $J$ is the system inertia matrix, $\Omega$ is the system angular velocity vector, $\Omega = [\omega_1\ \omega_2\ \omega_3]^\top$, $\boldsymbol{\tau_g}$ is the torque due to the Moon's gravity, and $\boldsymbol{\tau_a}$ is the control torque due to the gimbaled thruster. $\boldsymbol{\Phi} = [\alpha\ \phi\ \gamma]^\top$ and $W$ is given as

$$W = \begin{bmatrix} 1 & 0 & -s_\phi \\ 0 & c_{(\alpha+\theta)} & s_{(\alpha+\theta)}c_\phi \\ 0 & -s_{(\alpha+\theta)} & c_{(\alpha+\theta)}c_\phi \end{bmatrix} \tag{8}$$

It is to be noted that $J$ in Eq. (7) includes the inertia of the thruster. The effect of the attitude dynamics of the thruster on the lander attitude motion is neglected as the moment of inertia of the thruster is assumed to be very small compared to the moment of inertia of the lander. Furthermore, the measurement of the system angular velocity $\Omega$ is not available while the measurements of all other states in the system translational and rotational models, Eqs. (3)–(6) are available.

### 2.1. External disturbances

The external disturbances considered in this study are due to the Moon's gravity. The force due to the Moon's gravity is expressed as

$$\boldsymbol{F_g} = -\frac{m\mu}{(r^2 + x^2)^{3/2}}[x\ r\ 0]^\top \tag{9}$$

where $\mu$ is the Moon's gravitational parameter.

The torque due to the Moon's gravity is given by [15]

$$\boldsymbol{\tau_g} = 3\frac{\mu}{\|\boldsymbol{p}\|^3} R\hat{\boldsymbol{p}} \times (JR\hat{\boldsymbol{p}}) \tag{10}$$

where $\hat{\boldsymbol{p}} = \boldsymbol{p}/\|\boldsymbol{p}\|$. Expressing $\hat{\boldsymbol{p}}$ in terms of the coordinates of the inertial frame $O - X_iY_iZ_i$ as $\hat{\boldsymbol{p}} = -[x\ r\ 0]^\top \cdot 1/(x^2+r^2)^{1/2}$ and substituting it into (10) yields

$$\boldsymbol{\tau_g} = 3\frac{\mu}{\|\boldsymbol{p}\|^5} R[x\ r\ 0]^\top \times (JR[x\ r\ 0]^\top) \tag{11}$$

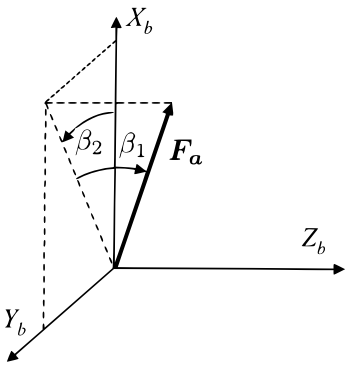


**Fig. 4.** Gimbaled thruster force vector.

### 2.2. Gimbaled thruster

The lander is provided with a gimbaled thruster having a variable thrust, $F$ and two control angles, $\beta_1$ and $\beta_2$ (Fig. 4). The position of the thruster is defined by a vector $\chi = [\chi_x\ \chi_y\ \chi_z]^\top$ with respect to the lander body-fixed frame, $S - X_bY_bZ_b$. The thruster force vector $\boldsymbol{F_a}$ is obtained as

$$\boldsymbol{F_a} = \begin{bmatrix} Fc_{\beta_1}c_{\beta_2} \\ Fc_{\beta_1}s_{\beta_2} \\ Fs_{\beta_1} \end{bmatrix} \tag{12}$$

with $F = \|\boldsymbol{F_a}\|$, $\beta_1$ is the angle over the $X_bY_b$ plane, and $\beta_2$ is the elevation angle towards $Z_b$ (see Fig. 4).

The resulting torque due to the thruster force vector is derived as $\boldsymbol{\tau_a} = \chi \times \boldsymbol{F_a}$, which yields to

$$\boldsymbol{\tau_a} = \begin{bmatrix} F\left(\chi_y s_{\beta_1} - \chi_z c_{\beta_1} s_{\beta_2}\right) \\ F\left(\chi_z c_{\beta_1} c_{\beta_2} - \chi_x s_{\beta_1}\right) \\ F\left(\chi_x c_{\beta_1} s_{\beta_2} - \chi_y c_{\beta_1} c_{\beta_2}\right) \end{bmatrix} \tag{13}$$

Consider the thruster position measured from the lander's center of mass as $\chi = [-l\ 0\ 0]^\top$ in the lander body frame, $l > 0$. The resulting torque due to the thruster is given by

$$\boldsymbol{\tau_a} = F\begin{bmatrix} 0 \\ ls_{\beta_1} \\ -lc_{\beta_1}s_{\beta_2} \end{bmatrix} \tag{14}$$

## 3. Controller design

The objective of the controller is to track a desired decent path to reach the target landing site for an unknown lander's mass without its angular velocity measurement. Two observers are designed to estimate the lander's mass and angular velocity followed by the design of the control law based on sliding mode control (SMC) technique [16]. A high order filter is developed to cater for non-affine control inputs. The SMC adds robustness against uncertainties and disturbances.

### 3.1. System mass observer design

The mass observer is designed based on the Immersion and Invariance approach [17], wherein an estimation error is a function of estimator's states, measured signals, and control inputs, and is defined as follows:

$$\tilde{m}_i = m_i - k_m[1 + \tanh(\hat{m}_i - \beta(\boldsymbol{v_c}, \boldsymbol{F_a}))] \tag{15}$$

where $m_i = 1/m$, $\boldsymbol{v_c} = [\dot{x}, \dot{r}, \dot{\theta}]^\top$, and the control input $\boldsymbol{F_a}$ is expressed in local coordinates. $k_m > 0$ is a constant, and $\beta(\boldsymbol{v_c}, \boldsymbol{F_a})$ is a scalar function explicitly defined by the following derivation. Taking the time derivative of (15) and using the fact that $\dot{\boldsymbol{v}}_c = \boldsymbol{a_c}$ we have

$$\begin{aligned} \dot{\tilde{m}}_i = -k_{m2}\Big\{ & \dot{\hat{m}}_i - \nabla_{\boldsymbol{v_c}}\beta\{\tilde{m}_i + k_m[1 + \tanh(\hat{m}_i - \beta)]\} \\ & \times (-\boldsymbol{F_g} + R^\top \boldsymbol{F_a}) - \nabla_{\boldsymbol{F_a}}\beta\dot{\boldsymbol{F}}_{\boldsymbol{a}}\Big\} \end{aligned} \tag{16}$$

with $k_{m2} = k_m[1 - \tanh(\hat{m}_i - \beta)^2]$. Arranging the terms for $\tilde{m}_i$ and $\hat{m}_i$, respectively in Eq. (16), we have the following two equations:

$$\begin{aligned} \dot{\tilde{m}}_i &= k_{m2}\nabla_{\boldsymbol{v_c}}\beta\tilde{m}_i(-\boldsymbol{F_g} + R^\top \boldsymbol{F_a}) \\ \dot{\hat{m}}_i &= \nabla_{\boldsymbol{v_c}}\beta k_m\{1 + \tanh(\hat{m}_i - \beta)\}(-\boldsymbol{F_g} + R^\top \boldsymbol{F_a}) + \nabla_{\boldsymbol{F_a}}\beta\dot{\boldsymbol{F}}_{\boldsymbol{a}}. \end{aligned}$$

From the preceding equation, the solution for $\beta$ such that $\tilde{m}_i \to 0$ is obtained as follows:

$$\beta = -k_\beta(-\boldsymbol{F_g} + R^\top \boldsymbol{F_a})^\top \boldsymbol{v_c}, \tag{17}$$

with $k_\beta$ as a positive gain constant, and the mass observer $\hat{m}$ can be derived as

$$\hat{m} = \left\{k_m\left[1 + \tanh(\hat{m}_i + k_\beta(-\boldsymbol{F_g} + R^\top \boldsymbol{F_a})^\top \boldsymbol{v_c})\right]\right\}^{-1} \tag{18}$$

where $\hat{m}_i$ is given by

$$\begin{aligned} \hat{m}_i = \int_0^t & -k_\beta(-\boldsymbol{F_g} + R^\top \boldsymbol{F_a})^\top(-\boldsymbol{F_g} + R^\top \boldsymbol{F_a}) \cdot \\ & \left[1 + \tanh(\hat{m}_i - \beta) - k_\beta \boldsymbol{v_c}^\top(R^\top \dot{\boldsymbol{F}}_{\boldsymbol{a}})\right] dt \end{aligned} \tag{19}$$

### 3.2. System angular velocity observer design

Here an angular velocity observer is designed based on the 'broken' super twisting sliding mode observer (SMO) design technique [18,19]. The observer estimates the lander's angular velocity for given measurement of Lander's attitude (Euler angles). It is designed as follows:

$$\begin{aligned} \dot{\hat{\boldsymbol{\Phi}}} &= W^{-1}(\hat{\boldsymbol{\Phi}})\hat{\Omega} + \zeta_{o1} \\ \dot{\hat{\Omega}} &= J^{-1}(J\hat{\Omega} \times \hat{\Omega} + \boldsymbol{\tau_a}) + \zeta_{o2} \\ \zeta_{o1} &= \lambda_o\sqrt{\left\|\boldsymbol{\Phi} - \hat{\boldsymbol{\Phi}}\right\|}\,\mathrm{sgn}(\boldsymbol{\Phi} - \hat{\boldsymbol{\Phi}}) \\ \zeta_{o2} &= \alpha_o\,\mathrm{sgn}(\boldsymbol{\Phi} - \hat{\boldsymbol{\Phi}}) \end{aligned} \tag{20}$$

where $\hat{\boldsymbol{\Phi}}$ and $\hat{\Omega}$ are the estimated Euler angles and angular rates, respectively; $\zeta_{o1}$ and $\zeta_{o2}$ are the observer correction variables; and $\lambda_o$ and $\alpha_o$ are the observer gains which make the observer converge to the true state of the system under Lyapunov conditions given by [19]

$$\begin{aligned} \alpha_o &> \epsilon \\ \lambda_o &> \sqrt{\tfrac{2}{\alpha_o - \epsilon}\tfrac{(\alpha_o + \epsilon)(1 + k_o)}{(1 - k_o)}} \end{aligned} \tag{21}$$

where

$$\begin{aligned} \epsilon &> \left\|J^{-1}(J\Omega \times \Omega - J\hat{\Omega} \times \hat{\Omega} + \boldsymbol{\tau_g}(\boldsymbol{\Phi}))\right\| \\ 0 &< k_o < 1 \end{aligned}$$

It is to be noted that the switching function $\mathrm{sgn}(x)$ in Eq. (21) is a sign function, which for implementation purposes and to avoid the problem of jitter, is replaced by $\tanh(x/\delta_o)$ with $\delta_o > 0$.

### 3.3. Control law design

We consider the reference state vector as follows:

$$\begin{bmatrix} x \\ r \\ \theta \end{bmatrix} = \begin{bmatrix} x_r \\ r_r \\ \theta_r \end{bmatrix}, \begin{bmatrix} \dot{x} \\ \dot{r} \\ \dot{\theta} \end{bmatrix} = \begin{bmatrix} \dot{x}_r \\ \dot{r}_r \\ \dot{\theta}_r = 0 \end{bmatrix}, \begin{bmatrix} \alpha \\ \phi \\ \gamma \end{bmatrix} = \begin{bmatrix} \alpha_r \\ \phi_r = 0 \\ \gamma_r \end{bmatrix}, \begin{bmatrix} \omega_1 \\ \omega_2 \\ \omega_3 \end{bmatrix} = \begin{bmatrix} \omega_{1r} = 0 \\ \omega_{2r} = 0 \\ \omega_{3r} = 0 \end{bmatrix} \tag{22}$$

where the subscript $r$ refers to the reference state. The control inputs at the reference state are chosen to sustain the hover flight as

$$\begin{bmatrix} F \\ \beta_1 \\ \beta_2 \end{bmatrix} = \begin{bmatrix} F_r = F_g[x_r\ r_r\ 0] \\ 0 \\ 0 \end{bmatrix} \tag{23}$$

Based on (22) and (23), the dynamic model (3) to (7) can be re-stated in terms of error coordinates defining $\tilde{\xi} = \xi - \xi_r$, where $\xi$ is any state variable or any control input:

$$\left.\begin{aligned}
\ddot{\tilde{x}} &= \frac{1}{m} e_1^{\top} \boldsymbol{F}_g(\tilde{x}, \tilde{r}) + \frac{1}{m} e_1^{\top} R^{\top}(\tilde{\boldsymbol{\Phi}}) \boldsymbol{F}_a(\tilde{F}, \tilde{\beta}_1, \tilde{\beta}_2) - \ddot{x}_r \\
\ddot{\tilde{r}} &= \frac{1}{m} e_2^{\top} \boldsymbol{F}_g(\tilde{x}, \tilde{r}) + (\tilde{r} + r_r)(\dot{\tilde{\theta}} + \dot{\theta}_r)^2 + \frac{1}{m} e_2^{\top} R^{\top}(\tilde{\boldsymbol{\Phi}}) \boldsymbol{F}_a(\tilde{F}, \tilde{\beta}_1, \tilde{\beta}_2) - \ddot{r}_r \\
\ddot{\tilde{\theta}} &= \frac{-2(\dot{\tilde{r}} + \dot{r}_r)(\dot{\tilde{\theta}} + \dot{\theta}_r)}{\tilde{r} + r_r} + \frac{1}{m(\tilde{r} + r_r)} e_3^{\top} R^{\top}(\tilde{\boldsymbol{\Phi}}) \boldsymbol{F}_a(\tilde{F}, \tilde{\beta}_1, \tilde{\beta}_2) - \ddot{\theta}_r \\
\dot{\tilde{\boldsymbol{\Phi}}} &= -e_1(\dot{\tilde{\theta}} + \dot{\theta}_r) + W^{-1}(\tilde{\boldsymbol{\Phi}})(\tilde{\Omega} + \Omega_r) - \dot{\boldsymbol{\Phi}}_r \\
\dot{\tilde{\Omega}} &= J^{-1}([J\tilde{\Omega} + \Omega_r)] \times (\tilde{\Omega} + \Omega_r) + \boldsymbol{\tau}_g(\tilde{\Omega}, \tilde{\boldsymbol{\Phi}}) + \boldsymbol{\tau}_a(\tilde{F}, \tilde{\beta}_1, \tilde{\beta}_2) - \dot{\Omega}_r
\end{aligned}\right\} \tag{24}$$

Linearizing (24) with respect to the reference state vector (22) and neglecting second and higher order terms, $\ddot{x}_r$, $\ddot{r}_r$, and two control inputs simultaneously affecting a state variable for simplicity (i.e., $\tilde{\beta}_1$ and $\tilde{\beta}_2$ affecting $\ddot{\tilde{r}}$ and $\ddot{\tilde{\theta}}$), we obtain the system equations of motion in linear form as follows:

$$\begin{bmatrix} \ddot{\tilde{x}} \\ \ddot{\tilde{r}} \\ \ddot{\tilde{\theta}} \end{bmatrix} = \frac{1}{m} K_{re} \begin{bmatrix} \tilde{F} \\ F_r(\tilde{\gamma} c_{\alpha_r} + \tilde{\phi} s_{\alpha_r}) \\ F_r(\tilde{\gamma} s_{\alpha_r} - \tilde{\phi} c_{\alpha_r}) \end{bmatrix} \tag{25}$$

$$\dot{\tilde{\boldsymbol{\Phi}}} = -e_1 \dot{\tilde{\theta}} + I \tilde{\Omega} \tag{26}$$

$$\dot{\tilde{\Omega}} = J^{-1} F_r \begin{bmatrix} 0 \\ \tilde{\beta}_1 \\ -\tilde{\beta}_2 \end{bmatrix} \tag{27}$$

where

$$K_{re} = \begin{bmatrix} 1 & 0 & 0 \\ 0 & 1 & 0 \\ 0 & 0 & 1/r_r \end{bmatrix}.$$

**Remark 1.** Since $1/r_r$ could be singular or could have large variations for small $r$, it is important to assume that $\|r_T - r_0\| \ll r_r$ for a given initial condition $r_0$ and a target position $r_T$, such that $r_r \in (r_0, r_T)$.

Next, the state variables are rearranged with respect to the separation of actuated and unactuated parts, defining $\tilde{X}_1 = [\tilde{x}\ \tilde{r}\ \tilde{\theta}\ \dot{\tilde{r}}\ \dot{\tilde{\theta}}\ \tilde{\alpha}\ \tilde{\phi}\ \tilde{\gamma}\ \tilde{\omega}_1]^{\top}$ as the unactuated states and $\tilde{X}_2 = [\dot{\tilde{x}}\ \tilde{\omega}_2\ \tilde{\omega}_3]^{\top}$ as the actuated states. Using (25), (26), and (27), the system equations of motion can be rewritten in the following form:

$$\begin{aligned} \dot{\tilde{X}}_1 &= A_{11}(\tilde{X}_1)\tilde{X}_1 + A_{12}\tilde{X}_2 \\ \dot{\tilde{X}}_2 &= B_2 \tilde{U}. \end{aligned} \tag{28}$$

where $A_{11}(\tilde{X}_1) \in \mathbb{R}^{9\times 9}$ is a nonlinear analytical matrix which is function of $\tilde{X}_1$, and $A_{12} \in \mathbb{R}^{9\times 3}$, $B_2 \in \mathbb{R}^{3\times 3}$ are constant linear matrices as

$$A_{11} = \left[\begin{array}{c|c|ccc|c} 0_{3\times 4} & 0_{3\times 1} & \multicolumn{3}{c|}{I_3} & 0_{3\times 1} \\ \hline 0_{1\times 4} & 0 & 0 & \Lambda_1 & \Lambda_2 & 0 \\ 0_{1\times 4} & 0 & 0 & \Lambda_3 & \Lambda_4 & 0 \\ \hline & -1 & \multicolumn{3}{c|}{} & 1 \\ 0_{3\times 4} & 0 & \multicolumn{3}{c|}{0_3} & 0 \\ & 0 & \multicolumn{3}{c|}{} & 0 \\ \hline 0_{1\times 4} & 0 & \multicolumn{3}{c|}{0_{1\times 3}} & 0 \end{array}\right],$$

$$A_{12} = \left[\begin{array}{ccc} 1 & 0 & 0 \\ \hline & 0_{5\times 3} & \\ \hline 0 & 1 & 0 \\ 0 & 0 & 1 \\ 0 & 0 & 0 \end{array}\right], \quad B_2 = \begin{bmatrix} 1/m & 0 & 0 \\ 0 & F_r/J_y & 0 \\ 0 & 0 & -F_r/J_z \end{bmatrix}, \tag{29}$$

where $I_3$, $0_{i\times j} \in \mathbb{R}^{i\times j}$ are the identity matrix and a matrix with all elements equal to zero, respectively. The terms $\Lambda_i$, $i = 1, 2, \ldots, 4$, are defined as

$$\begin{bmatrix} \Lambda_1 & \Lambda_2 \\ \Lambda_3 & \Lambda_4 \end{bmatrix} = \frac{F_r}{m} \begin{bmatrix} 0 & 1 \\ -1/r_r & 0 \end{bmatrix} R_{\alpha}^{\top} \tag{30}$$

with

$$R_{\alpha}^{\top} = \begin{bmatrix} c_{\alpha_r} & -s_{\alpha_r} \\ s_{\alpha_r} & c_{\alpha_r} \end{bmatrix}$$

And

$$\tilde{U} = \begin{bmatrix} \tilde{F} \\ \tilde{\beta}_1 \\ \tilde{\beta}_2 \end{bmatrix}, \tag{31}$$

### 3.3.1. Control design for unactuated states

We proceed to do a change of variables to system (28)

$$\begin{bmatrix} \tilde{\phi}_L \\ \tilde{\gamma}_L \end{bmatrix} = R_{\alpha}^{\top} \begin{bmatrix} \tilde{\phi} \\ \tilde{\gamma} \end{bmatrix} \tag{32}$$

taking the time derivative of (32) and considering $\dot{\alpha}_r = 0$, we have

$$\begin{bmatrix} \dot{\tilde{\phi}} \\ \dot{\tilde{\gamma}} \end{bmatrix} = R_{\alpha} \begin{bmatrix} \dot{\tilde{\phi}}_L \\ \dot{\tilde{\gamma}}_L \end{bmatrix} \tag{33}$$

Note that, from model (28) we have the relationship $\tilde{\omega}_2 = \dot{\tilde{\phi}}$ and $\tilde{\omega}_3 = \dot{\tilde{\gamma}}$. So, $\dot{\tilde{\phi}}_L = \tilde{\omega}_{2L}$ and $\dot{\tilde{\gamma}}_L = \tilde{\omega}_{3L}$, and Eq. (33) becomes

$$\begin{bmatrix} \tilde{\omega}_2 \\ \tilde{\omega}_3 \end{bmatrix} = R_{\alpha} \begin{bmatrix} \tilde{\omega}_{2L} \\ \tilde{\omega}_{3L} \end{bmatrix}$$

and we define $\tilde{X}_{2L}$ in terms of $\tilde{X}_2$ in (28) as

$$\begin{aligned} \tilde{X}_{2L} = \begin{bmatrix} \dot{\tilde{x}} \\ \tilde{\omega}_{2L} \\ \tilde{\omega}_{3L} \end{bmatrix} &= \begin{bmatrix} 1 & 0_{1\times 2} \\ 0_{2\times 1} & R_{\alpha}^{\top} \end{bmatrix} \tilde{X}_2 \\ &= R_x(\alpha)^{\top} \tilde{X}_2 \end{aligned} \tag{34}$$

the system (28) becomes

$$\begin{aligned} \dot{\tilde{X}}_{1L} &= A_{11L}\tilde{X}_{1L} + A_{12L}\tilde{X}_{2L} \\ \dot{\tilde{X}}_{2L} &= B_2 \tilde{U} \end{aligned} \tag{35}$$

with $\tilde{X}_{1L} = [\tilde{x}\ \tilde{r}\ \tilde{\theta}\ \dot{\tilde{r}}\ \dot{\tilde{\theta}}\ \tilde{\alpha}\ \tilde{\phi}_L\ \tilde{\gamma}_L\ \tilde{\omega}_1]^{\top}$ as the unactuated states and $\tilde{X}_{2L} = [\dot{\tilde{x}}\ \tilde{\omega}_{2L}\ \tilde{\omega}_{3L}]^{\top}$ as the actuated states,

$$A_{11L} = \left[\begin{array}{c|c|ccc|c} 0_{3\times 4} & 0_{3\times 1} & \multicolumn{3}{c|}{I_3} & 0_{3\times 1} \\ \hline 0_{1\times 4} & 0 & 0 & 0 & \frac{F_r}{m} & 0 \\ 0_{1\times 4} & 0 & 0 & -\frac{F_r}{mr_r} & 0 & 0 \\ \hline & -1 & \multicolumn{3}{c|}{} & 1 \\ 0_{3\times 4} & 0 & \multicolumn{3}{c|}{0_3} & 0 \\ & 0 & \multicolumn{3}{c|}{} & 0 \\ \hline 0_{1\times 4} & 0 & \multicolumn{3}{c|}{0_{1\times 3}} & 0 \end{array}\right],$$

and $A_{12L} = A_{12}$. Let us consider $\tilde{X}_{2L}$ as virtual control input in (35). In this particular case, the controllability matrix for the pair $(A_{11L}, A_{12L})$ has rank 7. A transformation is carried out in order to obtain a separation of controllable and uncontrollable states and then a technique is applied to stabilize the controllable states, let us define the transformation $T$ such that $\tilde{Z} = T\tilde{X}_{1L}$, with $\tilde{Z} \in \mathbb{R}^9$, we obtain a system of the form

$$\dot{\tilde{Z}} = \bar{A}\tilde{Z} + \bar{B}\tilde{X}_{2L} \tag{36}$$

where

$$\bar{A} = TA_{11L}T^{-1} = \begin{bmatrix} \bar{A}_{uc} & 0 \\ \bar{A}_{21} & \bar{A}_c \end{bmatrix}, \quad \bar{B} = TA_{12L}$$

$$T = \begin{bmatrix} 0 & 0 & 1/2 & 0 & 0 & 1/2 & 0 & 0 & -1/\sqrt{2} \\ 0 & 0 & 1/2 & 0 & 0 & 1/2 & 0 & 0 & 1/\sqrt{2} \\ 0 & 1 & 0 & 0 & 0 & 0 & 0 & 0 & 0 \\ 0 & 0 & 1/\sqrt{2} & 0 & 0 & -1/\sqrt{2} & 0 & 0 & 0 \\ 0 & 0 & 0 & 0 & -1 & 0 & 0 & 0 & 0 \\ 0 & 0 & 0 & -1 & 0 & 0 & 0 & 0 & 0 \\ 0 & 0 & 0 & 0 & 0 & 0 & 0 & 1 & 0 \\ 0 & 0 & 0 & 0 & 0 & 0 & -1 & 0 & 0 \\ 1 & 0 & 0 & 0 & 0 & 0 & 0 & 0 & 0 \end{bmatrix},$$

$$\bar{A}_{uc} = \begin{bmatrix} 2^{-3/2} & -2^{-3/2} \\ 2^{-3/2} & -2^{-3/2} \end{bmatrix}, \bar{A}_{21} = \begin{bmatrix} 0 & & 0 \\ -1/2 & & 1/2 \\ & 0_{5\times 2} & \end{bmatrix},$$

$$\bar{A}_c = \begin{bmatrix} 0 & 0 & 0 & -1 & 0 & 0 & 0 \\ 0 & 0 & \sqrt{2} & 0 & 0 & 0 & 0 \\ 0 & 0 & 0 & 0 & 0 & -\frac{F_r}{mr_r} & 0 \\ 0 & 0 & 0 & 0 & -\frac{F_r}{m} & 0 & 0 \\ & & & 0_{3\times 7} & & & \end{bmatrix}.$$

The controllability matrix for this system has rank equal to 7, which means that the system has 7 controllable states defined as $[\ \tilde{z}_3 \dots \tilde{z}_9\ ]^\top = \hat{T}\tilde{X}_{1L}$, with $\tilde{z}_3 = \tilde{r}$, $\tilde{z}_4 = (\tilde{\theta} - \tilde{\alpha}/\sqrt{2})$, $\tilde{z}_5 = -\dot{\tilde{\theta}}$, $\tilde{z}_6 = -\dot{\tilde{r}}$, $\tilde{z}_7 = \gamma$, $\tilde{z}_8 = \phi$, and $\tilde{z}_9 = x$, where $\hat{T} = T(3:9, 1:9)$ is the transformation matrix for the controllable states only.

On the other hand, the uncontrollable states $[\ \tilde{z}_1\ \tilde{z}_2\ ]^\top$, are stable since $[\ \dot{\tilde{z}}_1\ \dot{\tilde{z}}_2\ ]^\top = \bar{A}_{uc}[\ \tilde{z}_1\ \tilde{z}_2\ ]^\top$ produce two eigenvalues equal to zero, thus spanning an equilibrium region [20]. If we consider that $\tilde{z}_1 = 1/2(\tilde{\alpha} + \tilde{\theta}) - \tilde{\omega}_1/\sqrt{2}$, and $\tilde{z}_2 = 1/2(\tilde{\alpha} + \tilde{\theta}) + \tilde{\omega}_1/\sqrt{2}$ we see that this result is consistent with the fact that there are not control inputs for $\tilde{\alpha}$ and $\tilde{\omega}_1$. It is inferred then that the system is stabilizable because the uncontrollable mode is stable and the unstable mode is controllable. For the controllable part, the matrix gain $K_{lqr} \in \mathbb{R}^{3\times 7}$ is computed based on linear quadratic regulator (LQR) algorithm such that the controllable system in close loop has its poles in the left part of the complex plane. The control law for (36) is stated as $\tilde{X}_{2L} = -K_{lqr}[\tilde{z}_3, \dots, \tilde{z}_9]^\top$. Applying the transformation $T$, the first equation of system (35) is Hurwitz with the following feedback:

$$\tilde{X}_{2L} = -K_{lqr}\hat{T}\tilde{X}_{1L}. \tag{37}$$

In other words, taking $\tilde{X}_2$ from (34) and substituting $\tilde{X}_{2L}$ from (37) we have a state feedback that allows the first equation of system (28) to be Hurwitz, i.e.

$$\tilde{X}_2 = R_x(\alpha)\tilde{X}_{2L} = -R_x(\alpha)K_{lqr}\hat{T}\tilde{X}_{1L}, \tag{38}$$

### 3.3.2. Sliding surface

From (38), and considering the term $B_2$ in (28) we define a sliding surface of the form

$$S = \{\tilde{X}_1 \in \mathbb{R}^9, \tilde{X}_2 \in \mathbb{R}^3 : K_a\tilde{X}_2 + R_x(\alpha)K_{lqr}\hat{T}\tilde{X}_1 = 0\} \tag{39}$$

with $K_a = diag\{k_1, k_2, k_3\}$, scalars $k_i > 0$. When the system is operating on the sliding surface, $\tilde{X}_2$ can be substituted from (39) into (28) to obtain a reduce model with a pair $(A_{11}, A_{12})$ being Hurwitz. The sliding manifold can be rewritten as

$$S = \Gamma\tilde{X} \tag{40}$$

$$\Gamma = \left[\ R_x(\alpha)K_{lqr}\hat{T}\ \middle|\ K_a\ \right] \tag{41}$$

It is to be noted that the sliding surface given by Eq. (41) is written in terms of a state vector separated into an actuated state vector $\tilde{X}_2$ and a nonactuated state vector $X_1$; in the following section however, the same sliding surface is renamed as $S_z$, and is built on a new order of the state vector. In this regard, the matrix $\Gamma$ in (41) is rewritten as a column vector given as follows: $c_i \in \mathbb{R}^3$, $i = 1, \dots, 12$, as follows

$$\Gamma = [c_1, \dots, c_{12}]_{3\times 12} \tag{42}$$

### 3.4. High order filter

In this section, a high order filter is developed to solve the problem of non-affine control inputs without linearizing the non-affine nonlinear system model given in Section 2. In Section 3.3.2 a sliding manifold was found for an affine control input $\tilde{U}$. That approach is considered to determine optimal gains of the sliding surface. The next step is to state a nonlinear high order filter in terms of a non-affine control input $U$ by using the control gains calculated for $\tilde{U}$. By increasing the order of the system, the control inputs can be extracted by first finding $U_d = dU/dt = [\dot{F}, \dot{\beta}_1, \dot{\beta}_2]^\top$ and then integrating it to determine the control input $U$. Thus, the control law in terms of the non-affine control inputs can be expressed as:

$$U = \begin{bmatrix} F \\ \beta_1 \\ \beta_2 \end{bmatrix} = \int_0^t U_d\, d\tau \tag{43}$$

where

$$U_d = -\Theta^{-1}(\eta\sigma + \psi) \tag{44}$$

$$\Theta = \frac{1}{\hat{m}}K_{1T}K_rR^\top J_T + K_{1R}J^{-1}J_R, \tag{45}$$

$$K_r = \begin{bmatrix} 1 & 0 & 0 \\ 0 & 1 & 0 \\ 0 & 0 & 1/r \end{bmatrix},$$

$$J_T = \begin{bmatrix} c_{\beta_1}c_{\beta_2} & -s_{\beta_1}c_{\beta_2}F & -c_{\beta_1}s_{\beta_2}F \\ c_{\beta_1}s_{\beta_2} & -s_{\beta_1}s_{\beta_2}F & c_{\beta_1}c_{\beta_2}F \\ s_{\beta_1} & c_{\beta_1}F & 0 \end{bmatrix} \tag{46}$$

$$J_R = \begin{bmatrix} 0 & 0 & 0 \\ s_{\beta_1} & c_{\beta_1}F & 0 \\ -c_{\beta_1}s_{\beta_2} & s_{\beta_1}s_{\beta_2}F & -c_{\beta_1}c_{\beta_2}F \end{bmatrix} \tag{47}$$

and $\eta$ is a positive constant, while $\psi \in \mathbb{R}^3$ is the robust term against disturbances and uncertainties. The terms $K_{1T}$, $K_{1R}$ are gain matrices which are obtained from a high-order sliding surface defined as

$$\sigma = \dot{S}_z + \zeta S_z \tag{48}$$

where $\zeta$ is a positive constant and

$$S_z = K_{1T}\tilde{z}_{1T} + K_{1R}\tilde{z}_{1R} + K_2\tilde{z}_2 \tag{49}$$

with $\tilde{z}_{1T} = [\dot{\tilde{x}}\ \dot{\tilde{r}}\ \dot{\tilde{\theta}}]^\top$, $\tilde{z}_{1R} = [\tilde{\omega}_1\ \tilde{\omega}_2\ \tilde{\omega}_3]^\top$, $\tilde{z}_2 = [\tilde{x}\ \tilde{r}\ \tilde{\theta}\ \tilde{\alpha}\ \tilde{\phi}\ \tilde{\gamma}]^\top$, $K_{1T} = [c_{10}, c_4, c_5]$, $K_{1R} = [c_9, c_{11}, c_{12}]$, and $K_{1R} = [c_1, c_2, c_3, c_6, c_7, c_8]$= with $c_i$ as defined in (42). It is to be noted that the purpose of rearranging the state variables in the sliding surface $S$ into $S_z$ is to separate the terms which have direct actuation of the control inputs, this is $\dot{\tilde{x}}\ \dot{\tilde{r}}\ \dot{\tilde{\theta}}$ for the translational states, $\tilde{\omega}_1\ \tilde{\omega}_2\ \tilde{\omega}_3$ for the rotational states, from the terms which do not have direct actuation of control inputs. Furthermore, considering practical implementation of the proposed control law given by Eq. (43), a rate of change in the control input must be limited. Therefore, a first-order low-pass filter is added to the control input with a cutoff frequency of 5 Hz.

**Remark 2.** The term $U_d$ in (44) becomes singular if $\Theta$ is not invertible. This condition holds if: (a) $r = 0$ which should be avoided in the definition of system coordinates; (b) $F = 0$ which represents a null action of the thruster. In this case, the controller is not used and the control torque and control force in the equations of motion are taken as null; the controller could be turned on again once $F \neq 0$.

**Remark 3.** In the control law it is required to have the values of $\dot{\Omega}$ and $\ddot{p}$ for the computation of high order sliding surface $\sigma$; these terms can be estimated by a high order sliding mode observer as in [21].

In order to determine the size of $\psi$ we take the worst case upper-bound of the disturbances [9].

$$\psi = \rho \left[\tanh\left(\frac{\rho\sigma_1}{\delta}\right), \tanh\left(\frac{\rho\sigma_2}{\delta}\right), \tanh\left(\frac{\rho\sigma_3}{\delta}\right)\right]^\top \tag{50}$$

where $\rho$ and $\delta$ are positive constants. The parameter $\delta$ is introduced as in [12,22] to avoid high frequency chattering at the expense of allowable loss of accuracy in the control signal [16].

### 3.5. Stability analysis

**Theorem 1.** *The model of the lunar lander with a single gimbal thruster given by Eqs. (2), (6) and (7) with the control law (44) and the high order filter (48), under the assumption that uncertainties and external disturbances are bounded, converges to the desired trajectory defined by a domain $\mathfrak{D}$ around the operational point ($\phi = \gamma = \beta_1 = \beta_2 = 0, r = r_r$), for a sufficiently small $\delta > 0$ given in (50) with*

$$\mathfrak{D} \triangleq \left[\sigma : \|\sigma\| \leq \sqrt{\frac{\delta}{2\eta(1+\delta_m)}}\right] \tag{51}$$

**Proof.** Let us define the following Lyapunov function candidate

$$V(\sigma) = \frac{1}{2}\sigma^\top\sigma + \frac{1}{2\gamma}\tilde{m}_i^2. \tag{52}$$

Taking the time derivative of $V(\sigma)$ we have

$$\begin{aligned}\dot{V}(\sigma) &= \sigma^\top\dot{\sigma} + \frac{1}{\gamma}\tilde{m}_i\dot{\hat{m}}_i \\ &= \sigma^\top\dot{\sigma} + \frac{1}{\gamma}\tilde{m}_i[-k_{m2}k_\beta(-F_g+U)^2]\tilde{m}_i\end{aligned}$$

The time derivative of $\sigma$ is

$$\begin{aligned}\dot{\sigma} = \ddot{S}_z + \zeta\dot{S}_z &= K_{1T}\dddot{z}_{1T} + K_{1R}\dddot{z}_{1R} + K_2\dddot{z}_2 \\ &+\zeta(K_{1T}\ddot{z}_{1T} + K_{1R}\ddot{z}_{1R} + K_2\ddot{z}_2)\end{aligned} \tag{53}$$

where $\dddot{z}_{1T} = [\dddot{x}\ \dddot{r}\ \dddot{\theta}]$, $\dddot{z}_{1R} = \dddot{\Omega}$ assuming that $\dddot{x}_d = \dddot{r}_d = \dddot{\theta}_d = 0$, $\dddot{\Omega}_d = 0$. Substituting these terms into (53) yields

$$\begin{aligned}\dot{\sigma} &= [K_{1T}\ K_{1R}][\dddot{x}\ \dddot{r}\ \dddot{\theta}\ \dddot{\Omega}]^\top + K_2\dddot{z}_2 \\ &+\zeta(K_{1T}\ddot{z}_{1T} + K_{1R}\ddot{z}_{1R} + K_2\ddot{z}_2).\end{aligned} \tag{54}$$

The terms $\dddot{x}, \dddot{r}, \dddot{\theta}$ and $\dddot{\Omega}$ in (54) may be computed analytically by taking the time derivatives of the equations of motion (3) to (5) and (7), respectively. From such derivatives, it is evident that some terms, such as $\dot{\boldsymbol{F}}_{\boldsymbol{a}}$ and $\dot{\boldsymbol{\tau}}_{\boldsymbol{a}}$ contain the time derivative of control inputs. Let us collect these terms as follows

$$\dot{\sigma} = K_{1T}\frac{1}{\hat{m}}K_r R^\top\dot{\boldsymbol{F}}_{\boldsymbol{a}} + K_{1R}J^{-1}\dot{\boldsymbol{\tau}}_{\boldsymbol{a}} + \Gamma_l \tag{55}$$

with

$$\begin{aligned}\Gamma_l &= [K_{1T}\ K_{1R}][r_a\ r_o]^\top + K_2\ddot{z}_2 \\ &+ \zeta(K_{1T}\ddot{z}_{1T} + K_{1R}\ddot{z}_{1R} + K_2\dot{z}_2) \\ r_a &= \frac{1}{\hat{m}}\left[\dot{\boldsymbol{F}}_{\boldsymbol{g}} + \frac{d}{dt}\begin{bmatrix}0\\ r\dot{\theta}^2\\ -2\dot{r}\dot{\theta}/r\end{bmatrix} + (\dot{K}_r R^\top + K_r\dot{R}^\top)\boldsymbol{F}_{\boldsymbol{a}}\right] \\ r_o &= J^{-1}\left(J\dot{\Omega}\times\Omega + J\Omega\times\dot{\Omega} + \dot{\boldsymbol{\tau}}_{\boldsymbol{g}}\right).\end{aligned}$$

The term $\Gamma_l$ represents the lumped terms corresponding to disturbances, low order terms in the sliding surface (53), and other derivative terms which do not contain $\dot{\boldsymbol{F}}_{\boldsymbol{a}}$ and $\dot{\boldsymbol{\tau}}_{\boldsymbol{a}}$. The estimated mass $\hat{m}$ is replaced by $m$. We can state the time derivative of input force, $\dot{\boldsymbol{F}}_{\boldsymbol{a}}$, and that of the input torque, $\dot{\boldsymbol{\tau}}_{\boldsymbol{a}}$, from (12) and (14), respectively as follows

$$\begin{aligned}\dot{\boldsymbol{F}}_{\boldsymbol{a}} &= \begin{bmatrix}c_{\beta_1}c_{\beta_2} & -s_{\beta_1}c_{\beta_2}F & -c_{\beta_1}s_{\beta_2}F\\ c_{\beta_1}s_{\beta_2} & -s_{\beta_1}s_{\beta_2}F & c_{\beta_1}c_{\beta_2}F\\ s_{\beta_1} & c_{\beta_1}F & 0\end{bmatrix}\begin{bmatrix}\dot{F}\\ \dot{\beta}_1\\ \dot{\beta}_2\end{bmatrix} \\ &= J_T U_d\end{aligned} \tag{56}$$

**Table 1**
Parameters of lander.

| Parameter | Symbol | Value |
|---|---|---|
| Mass | m | 100 kg |
| Moment of inertia | $J$ | diag{100, 90, 80} kg m$^2$ |
| Gravitational parameter | $\mu$ | $4.902\times10^{12}$ m$^3$/s$^2$ |
| Moon radius | $r_m$ | $1738\times10^3$ m |

$$\begin{aligned}\dot{\boldsymbol{\tau}}_{\boldsymbol{a}} &= \begin{bmatrix}0 & 0 & 0\\ s_{\beta_1} & c_{\beta_1}F & 0\\ -c_{\beta_1}s_{\beta_2} & s_{\beta_1}s_{\beta_2}F & -c_{\beta_1}c_{\beta_2}F\end{bmatrix}\begin{bmatrix}\dot{F}\\ \dot{\beta}_1\\ \dot{\beta}_2\end{bmatrix} \\ &= J_R U_d.\end{aligned} \tag{57}$$

Substituting $\dot{\sigma}$ from (55)–(57) into (53) and defining

$$\begin{aligned}a &= K_{1T}K_r R^\top J_T \\ b &= K_{1R}J^{-1}J_R \\ c &= k_{m2}k_\beta(-F_g+U)^2 \geq 0\end{aligned} \tag{58}$$

we have

$$\dot{V}(\sigma) = \sigma^\top[(\frac{a}{m}+b)U_d + \Gamma_l] - \frac{c}{\gamma}\tilde{m}_i^2. \tag{59}$$

Substituting the control law $U_d$ given by (44) into (59) yields to

$$\begin{aligned}\dot{V}(\sigma) &= \sigma^\top[-(\frac{a}{m}+b)(\frac{a}{\hat{m}}+b)^{-1}(\eta\sigma+\psi) + \Gamma_l] \\ &- \frac{c}{\gamma}\tilde{m}_i^2\end{aligned} \tag{60}$$

Taking $m = m_i^{-1}$ and substituting $m_i$ and $\hat{m}$ from (15) and (18), respectively, and defining $f(\hat{m}_i) = k_m(1+\tanh(\hat{m}_i + k_\beta(-F_g+U)^\top\dot{p}))$, we have

$$\begin{aligned}\dot{V}(\sigma) &= \sigma^\top\left[-\frac{(\tilde{m}_i + f(\hat{m}_i))a+b}{f(\hat{m}_i)a+b}(\eta\sigma+\psi) + \Gamma_l\right] - \frac{c}{\gamma}\tilde{m}_i^2 \\ &= \sigma^\top\left[-(\eta\sigma+\psi) + \Gamma_l\right] - \frac{c}{\gamma}\tilde{m}_i^2 - \frac{\tilde{m}_i a\sigma^\top(\eta\sigma+\psi)}{f(\hat{m}_i)a+b} \\ &\leq -\eta\sigma^\top\sigma + \delta - \frac{\eta}{\gamma}(\tilde{m}_i^2) - \frac{1}{\gamma}(c-\eta)\tilde{m}_i^2 \\ &- \frac{\tilde{m}_i a\sigma^\top(\eta\sigma+\psi)}{f(\hat{m}_i)a+b} \leq -2\eta V + \delta\end{aligned} \tag{61}$$

with the condition

$$-\frac{1}{\gamma}(c-\eta)\tilde{m}_i^2 - \frac{\tilde{m}_i a\sigma^\top(\eta\sigma+\psi)}{f(\hat{m}_i)a+b} \leq 0, \tag{62}$$

which holds for a given estimated $\tilde{m}_i$ and set of positive values $k_m, k_{m2}$, $k_\beta, \gamma$. Eq. (61) can be solved by comparison lemma as a differential equation of first order for the variable $V(t)$. The solution for the differential equation is found to be

$$V(t) \leq \frac{\delta}{2\eta} + (V(0) - \frac{\delta}{2\eta})e^{-2\eta t}. \tag{63}$$

Therefore, $\sigma$ is uniformly ultimately bounded, such that when $\sigma$ is outside of the set $\mathfrak{D}$, and inequality (62) holds, then $\dot{V}(\sigma) \leq 0$ and $\sigma$ converges to the set $\mathfrak{D}$ given in (51) [9]. □

## 4. Results and discussion

The parameters which define the lander characteristics are summarized in Table 1 [2]. The desired trajectory is assumed to be the straight line path and the corresponding desired state variables are given in Table 2. The system model given by Eqs. (2), (6) and (7) and the control law, Eq. (44) are numerically integrated using the 4th order Runge Kutta method with the step size of 0.001 s and the initial conditions given in Tables 3 and 4, respectively.

Table 5 presents the parameters used for the controller and observers as described in Section 3. The parameters $Q_{lqr}$ and $R_{lqr}$ in (38)

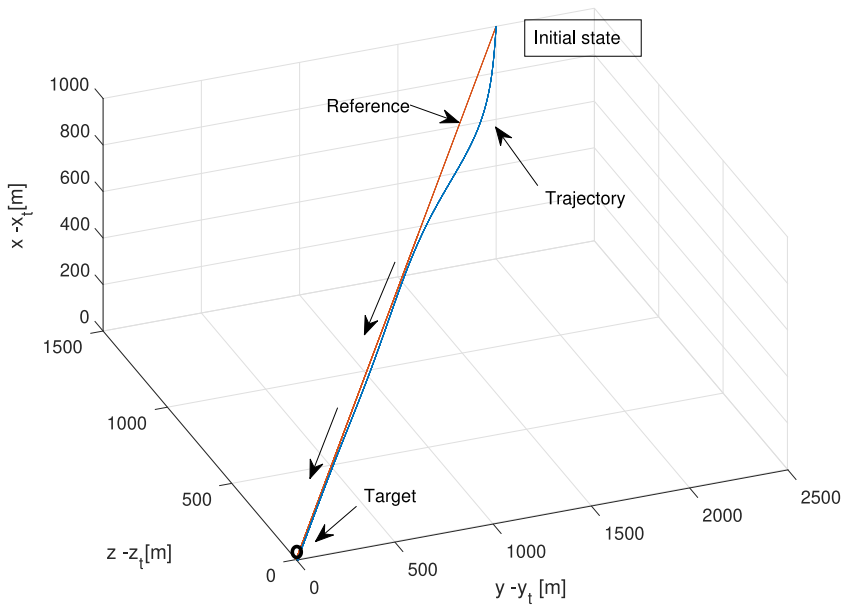


**Fig. 5.** Lander trajectory and reference trajectory.

**Table 2**
Desired trajectory, D = 200 s is the terminal time from beginning until the end of landing.

| Variable | Desired value |
|---|---|
| $x_d$ | $r_m + 1000(1 - \sin(\pi t/(2D)))$ [m] |
| $r_d$ | $2500(1 - \sin(\pi t/(2D)))$ [m] |
| $\theta_d$ | 0.6435 [rad] |
| $\alpha_d, \phi_d$ | 0 [rad] |
| $\gamma_d$ | $\arctan\left(\frac{\ddot{r}_d + \mu r_d/(x_d^2+r_d^2)^{3/2}}{\ddot{x}_d + \mu x_d/(x_d^2+r_d^2)^{3/2}}\right)$ [rad] |
| $\dot{x}_d$ | $-\pi/(2D)1000(\cos(\pi t/(2D)))$ [m/s] |
| $\dot{r}_d$ | $-\pi/(2D)2500(\cos(\pi t/(2D)))$ [m/s] |
| $\Omega_d$ | $[0\ 0\ 0]^\top$ [rad/s] |

**Table 3**
Initial state conditions.

| Variable | Value |
|---|---|
| $[x_0\ r_0\ \theta_0]$ | $[r_m + 1000\ \ 2500\ \ 0.6435]$ [m] |
| $[\alpha\ \phi\ \gamma]$ | [0 0 0] [rad] |
| $[\dot{x}_0\ \dot{r}_0\ \dot{\theta}_0]$ | $[-10\ \ -24\ \ -0.0028]$ [m/s] |
| $\Omega_0$ | [0 0 0] [rad/s] |

**Table 4**
Initial control input conditions.

| Variable | Value |
|---|---|
| $F(0)$ | 160 N |
| $\beta_1(0)$ | −0.02 rad |
| $\beta_2(0)$ | −0.001 rad |

**Table 5**
Control and observer parameters.

| Parameter | Value |
|---|---|
| $F_r$ | 160 N |
| $r_r$ | 10 000 m |
| $\rho$ | 1 |
| $\eta$ | 0.1 |
| $k_1, k_2, k_3$ | 5.0, 14.0, 2.0 respectively |
| $\delta$ | $5 \times 10^1$ |
| $\zeta$ | 2 |
| $k_m$ | 5 |
| $k_\beta$ | $1 \times 10^{-3}$ |
| $\lambda_o$ | 2 |
| $\alpha_o$ | 0.2 |
| $\delta_o$ | 0.01 |

**Table 6**
Noise parameters.

| State | $\sigma_s$ | $\sigma_{ns}$ |
|---|---|---|
| $x - x_T$ | 1 m | 2 % |
| $\dot{x}$ | 0.01 m/s | 2 % |
| $r - r_T$ | 1.4142 m | 2 % |
| $\dot{r}$ | 0.014142 m/s | 2 % |
| $\theta$ | $1 \times 10^{-4}$ rad | 2 % |
| $\dot{\theta}$ | $1 \times 10^{-6}$ rad/s | 2 % |
| $\boldsymbol{\Phi}$ | 0.1 rad each axis | 2 % |
| $\Omega$ | 0.01 rad/s each axis | 2 % |

are set as $Q_{lqr} = diag\{1\times10^2,\ 1\times10^9,\ 4\times10^{12},\ 1\times10^3,\ 7\times10^6,\ 7\times10^6,\ 1\times10^2\}$, $R_{lqr} = diag\{1\times10^3,\ 5\times10^6,\ 1\times10^8\}$. The gain matrix $K_{lqr}$ in Eq. (41) is obtained as

$$K_{lqr} = \begin{bmatrix} 0 & 0 & 0 & 0 & 0 & 0 & 0.3 \\ 0 & -14.1 & 1,063 & 0 & 0 & -1.3 & 0 \\ -0.001 & 0 & 0 & 0.02 & -0.3 & 0 & 0 \end{bmatrix}$$

Furthermore, the state measurement errors are also considered. We use Gaussian white noises [3] made up of a stationary error $\delta X_s$ and a non-stationary scale error $\delta X_{ns}$ such that the measured state space is $X_m = X(1 + \delta X_{ns}) + \delta X_s$, with $\delta X = [\delta x\ \delta r\ \delta\theta\ \delta\dot{x}\ \delta\dot{r}\ \delta\dot{\theta}\ \delta\boldsymbol{\Phi}\ \delta\Omega]$. The standard deviations for both errors are $\sigma_s$ and $\sigma_{ns}$, respectively and their mean values are zero in both cases (see Table 6 [2]). It is to be noted that the noises for $\theta$ and its derivative are simulated with a standard deviation of 2.0% of $(r - r_T)/r$ and $(r - r_T)/(100r)$, respectively.

Figs. 5–10 show the performance of the proposed control methodology. The trajectory of the lander follows the reference trajectory. It can be seen that although the initial conditions separate the lander from the desired trajectory, it finally converges to it and makes the touch down at the desired point of landing with position ($x$, $y$, $z$) and attitude ($\phi$, $\gamma$, $\alpha$) errors of $\Delta x = 0$ m, $\Delta y = 2.58$ m, and $\Delta z = 3.96$ m, $\Delta\phi = 0.35$ deg, $\Delta\gamma = 0.075$ deg, and $\Delta\alpha = 24.26$ deg, respectively. The attitude Euler angle rate errors at the target are $\Delta\dot{\phi} = 0.001$ deg/s, $\Delta\dot{\gamma} = 0.07$ deg/s, and $\Delta\dot{\alpha} = 0.06$ deg/s, respectively. It is to be noted that the yaw attitude $\alpha$ is not controlled at the target location; this is due to null yaw torque as the thruster gets aligned along the lander's yaw axis as it approaches the target.

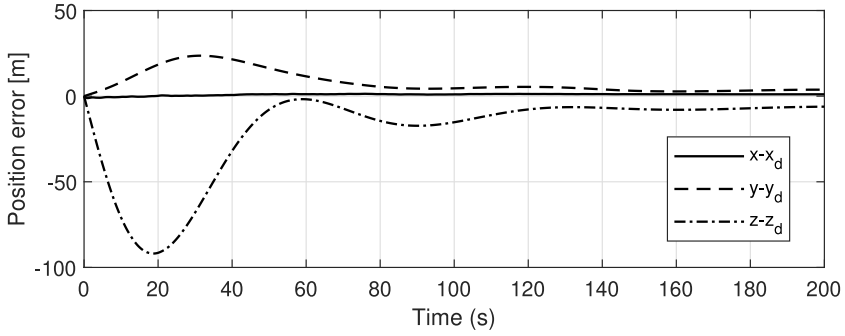


**Fig. 6.** Position errors (in Cartesian coordinates).

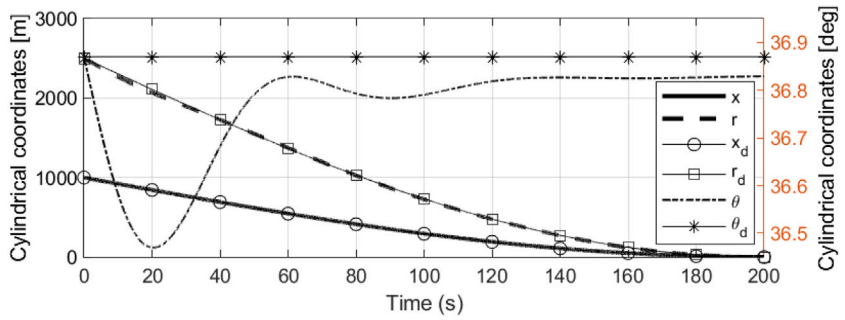


**Fig. 7.** Lander states: position ($x$, $r$, and $\theta$).

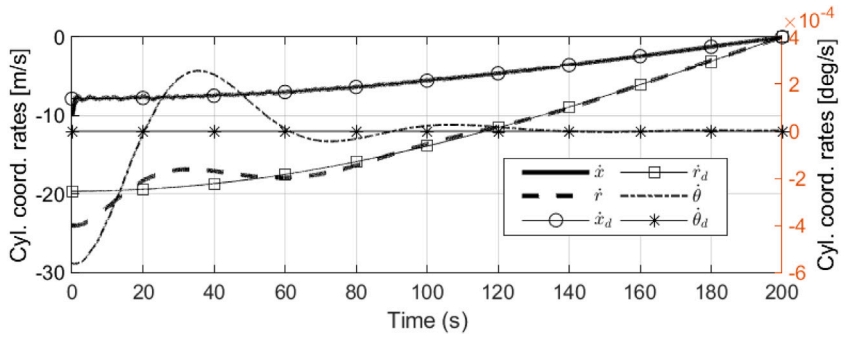


**Fig. 8.** Lander states: velocity ($\dot{x}$, $\dot{r}$, and $\dot{\theta}$).

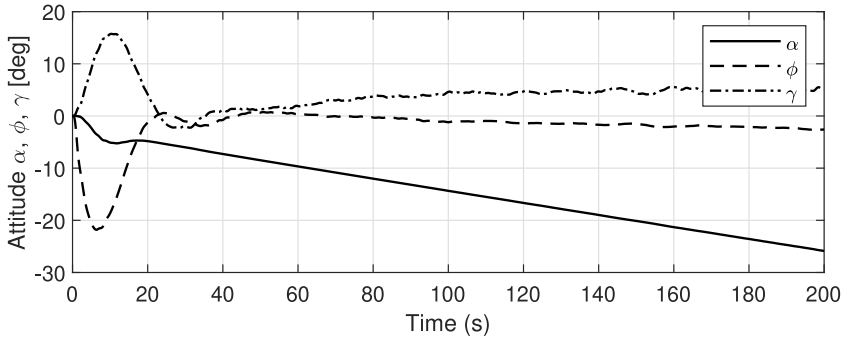


**Fig. 9.** Lander states: attitude ($\alpha$, $\phi$, $\gamma$).

The control input responses are shown in Figs. 11–13. The control force varies around its equilibrium value, $F_r = 160$ N while the gimbal angles reach null as the lander reaches the target. Furthermore, the control input responses do not have high frequency components as desired. Figs. 14 and 15 present the responses of the mass and angular rate observers, respectively.

*Monte Carlo simulation*

Next, the performance of the proposed control scheme is tested via Monte Carlo simulation wherein 50 simulations are carried out with variations in state measurement noise parameters following Table 6, and with initial state conditions as per Table 7. The normal distribution

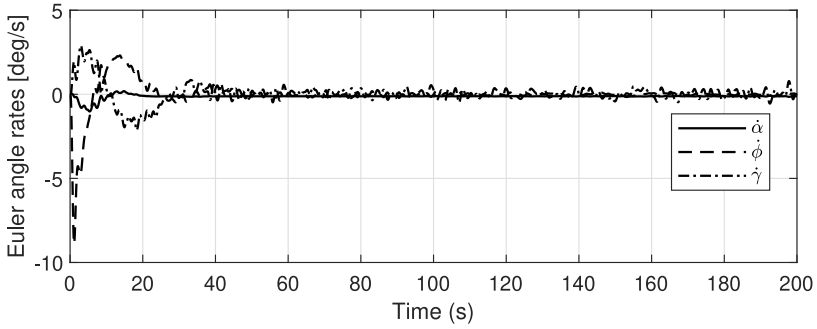


**Fig. 10.** Lander states: attitude rates ($\dot{\alpha}$, $\dot{\phi}$, $\dot{\gamma}$).

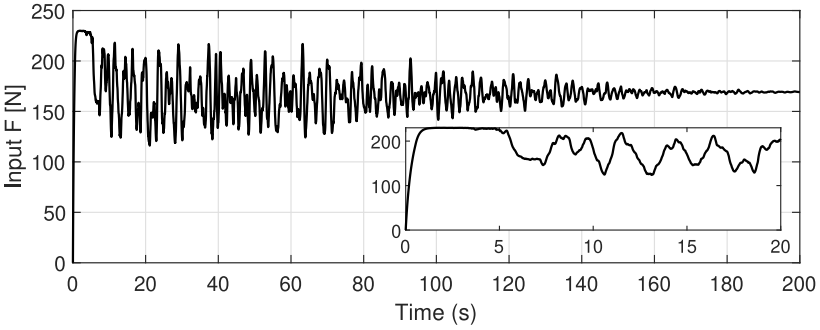


**Fig. 11.** Control input response.

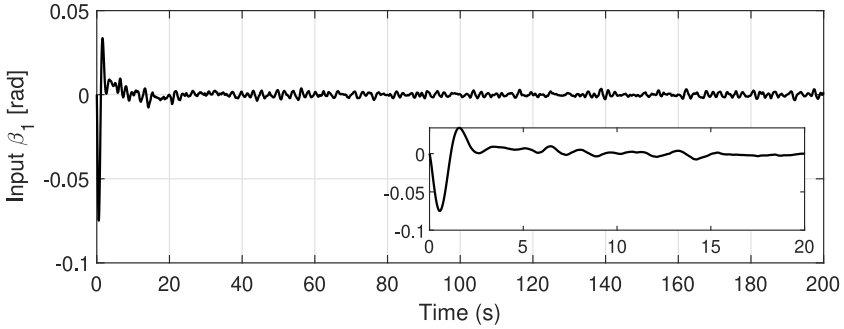


**Fig. 12.** Control input response.

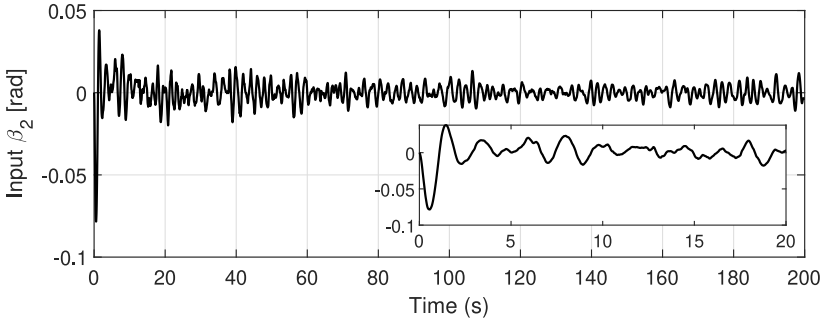


**Fig. 13.** Control input response.

of initial state conditions for each state $X$, is described by a mean value of $m_0$ and a standard deviation of $\sigma_0$. Figs. 16–19 show the results of the Monte Carlo simulation. For all cases considered here, the lander reaches the desired target within position ($x$, $y$, $z$) and attitude ($\phi$, $\gamma$) errors of $\Delta x$ = 2.54 m, $\Delta y$ = 9.53 m, and $\Delta z$ = 9.53 m, $\Delta\phi$ = 0.04 deg, and $\Delta\gamma$ = 0.015 deg, respectively. The lander angular rate errors for $\omega_2$ and $\omega_3$ at the target are within 0.002 deg/s and 0.005 deg/s, respectively. The responses for attitude angle $\alpha$ and angular rate $\omega_1$ are not presented as they incur large but bounded errors at the target position.

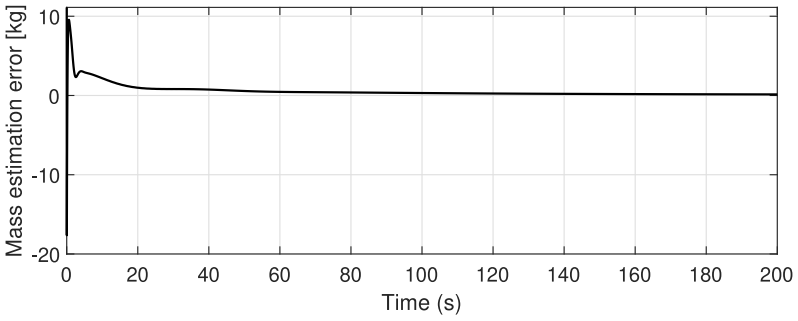


**Fig. 14.** Estimated mass error response.

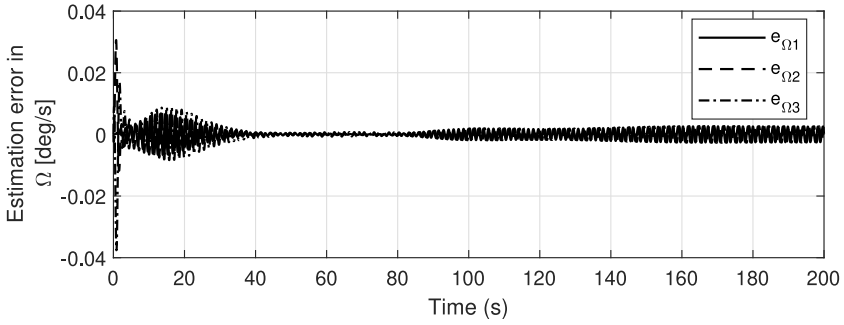


**Fig. 15.** Angular velocity estimation error response, $[e_{\Omega 1}\ e_{\Omega 2}\ e_{\Omega 3}]^{\mathrm{T}} = \Omega - \hat{\Omega}$.

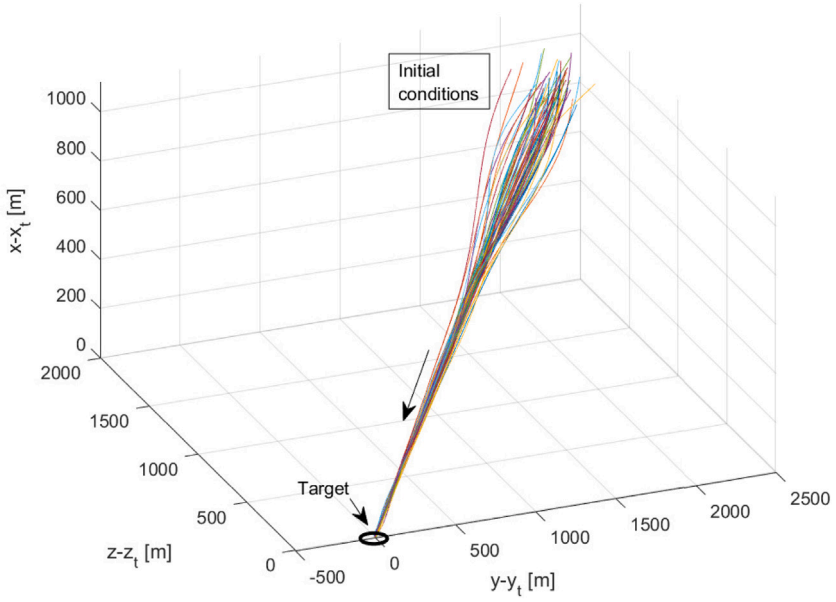


**Fig. 16.** Landing trajectory for different initial conditions.

**Table 7**
Normal distribution parameters of initial state conditions.

| State | $m_0$ | $\sigma_0$ |
|---|---|---|
| $x_0$ | 1 739 000, [m] | 50, [m] |
| $r_0$ | 12 600, [m] | 125, [m] |
| $\theta_0$ | .6435, [rad] | 0.005, [rad] |
| $\dot{x}_0$ | −10, [m/s] | 0.5, [m/s] |
| $\dot{r}_0$ | −20, [m/s] | 1, [m/s] |
| $\dot{\theta}_0$ | 0, [rad/s] | $2.8 \times 10^{-4}$, [rad/s] |
| $\boldsymbol{\Phi}_0$ | [0 0 0], [rad] | [0.01 0.05 0.05], [rad] |
| $\boldsymbol{\Omega}_0$ | [0 0 0], [rad/s] | [0 0.05 0.05], [rad/s] |

## 5. Conclusions

In this paper, the position and attitude control of a lunar lander using only a single thruster is examined. The thruster is considered to be double gimballed and three control inputs (thrust and two gimbal angles) are applied to control the six-degrees of freedom of the lunar lander with unknown mass and without angular velocity measurements. A nonlinear controller along with a mass and an angular velocity observers are designed. The Lyapunov theory is applied to prove the stability of the proposed control scheme. The results of the numerical simulations along with Monte Carlo simulations show that the lander reaches the desired target with required precision even in the

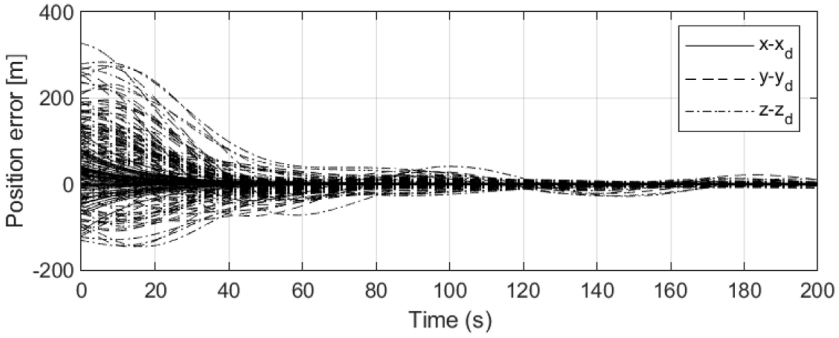


**Fig. 17.** Lander position errors (in Cartesian coordinates) for different initial conditions.

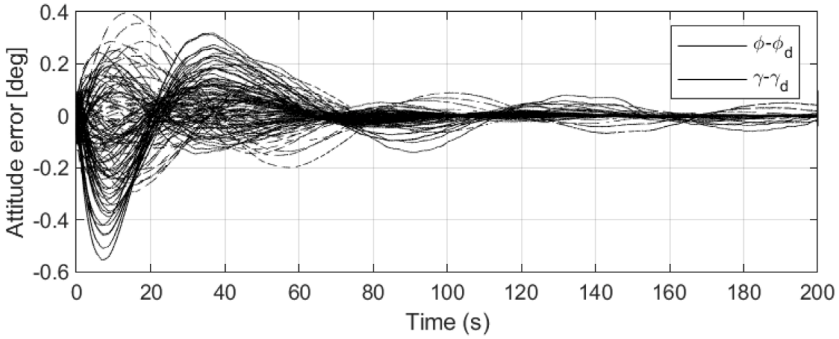


**Fig. 18.** Lander attitude errors for different initial conditions.

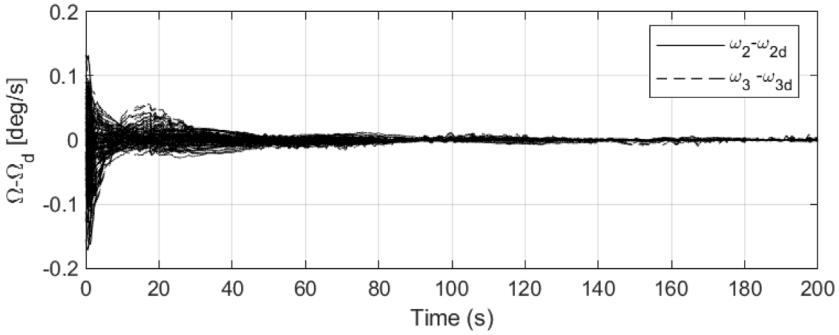


**Fig. 19.** Lander angular velocity rate errors for different initial conditions.

presence of sensor measurement noise and different initial conditions. This result is significant since it represents a valid opportunity for future missions, where the number of actuators onboard the lander is limited or only single thruster is available to control the lander. Successful implementation of this approach into an actual mission will greatly allow potentially overall mission cost reduction.

## Declaration of competing interest

The authors declare that they have no known competing financial interests or personal relationships that could have appeared to influence the work reported in this paper.

## Acknowledgment

The authors acknowledge the support of the Natural Sciences and Engineering Research Council of Canada (NSERC).

## References

[1] S. Li, X. Jiang, T. Tao, Guidance summary and assessment of the Chang'e-3 powered descent and landing, J. Spacecr. Rockets 53 (2) (2016) 258–277, http://dx.doi.org/10.2514/1.A33208.

[2] J.-W. Kwon, D. Lee, H. Bang, Virtual trajectory augmented landing control based on dual quaternion for Lunar Lander, J. Guid. Control Dyn. 39 (9) (2016) 2044–2057, http://dx.doi.org/10.2514/1.G001459.

[3] F. Zhang, G.-R. Duan, Integrated translational and rotational control for the terminal landing phase of a lunar module, Aerosp. Sci. Technol. 27 (1) (2013) 112–126, http://dx.doi.org/10.1016/j.ast.2012.07.003.

[4] B. Nagabhushan, G. Faiss, Thrust vector control of a V/STOL airship, J. Aircr. 21 (6) (1984) 408–413, http://dx.doi.org/10.2514/3.44980.

[5] Y. Ishijima, S. Matsumoto, K. Hayashi, Re-entry and terminal guidance for vertical-landing tsto (two-stage to orbit), in: Guidance, Navigation, and Control Conference and Exhibit, 1998, p. 4120, http://dx.doi.org/10.2514/6.1998-4120.

[6] X. Liu, Fuel-optimal rocket landing with aerodynamic controls, J. Guid. Control Dyn. 42 (1) (2018) 65–77, http://dx.doi.org/10.2514/1.G003537.

[7] W.S. Widnall, Lunar module digital autopilot, J. Spacecr. Rockets 8 (1) (1971) 56–62, http://dx.doi.org/10.2514/3.30217.

[8] M. Sagliano, M. Dumke, S. Theil, Simulations and flight tests of a new nonlinear controller for the EAGLE lander, J. Spacecr. Rockets 56 (1) (2019) 1–14, http://dx.doi.org/10.2514/1.A34161.

[9] Godard, K.D. Kumar, A.-M. Zou, A novel single thruster control strategy for spacecraft attitude stabilization, Acta Astronaut. 86 (2013) 55–67, http://dx.doi.org/10.1016/j.actaastro.2012.12.018.
[10] F.F. Saberi, M. Zandieh, Design and analysis of gimbal thruster configurations for 3-axis satellite attitude control, Int. J. Comput. Appl. 112 (6) (2015).
[11] A. Frias, A.H. de Ruiter, K.D. Kumar, Velocity-free attitude stabilization of a Nadir-Pointing underactuated rigid spacecraft, J. Guid. Control Dyn. 41 (5) (2017) 1068–1082, http://dx.doi.org/10.2514/1.G003281.
[12] Godard, K.D. Kumar, A. Zou, Robust stationkeeping and reconfiguration of underactuated spacecraft formations, Acta Astronaut. 105 (2) (2014) 495–510, http://dx.doi.org/10.1016/j.actaastro.2014.10.008.
[13] K.D. Kumar, Fundamentals of Dynamics and Control of Space Systems, second ed., Amazon Createspace Publishing, 2020.
[14] D.K. Geller, T.A. Lovell, Angles-only initial relative orbit determination performance analysis using cylindrical coordinates, J. Astronaut. Sci. 64 (1) (2017) 72–96, http://dx.doi.org/10.1007/s40295-016-0095-z.
[15] P.C. Hughes, Spacecraft Attitude Dynamics, Courier Corporation, 2012.
[16] T.A. Dwyer III, H. Sira-Ramirez, Variable-structure control of spacecraft attitude maneuvers, J. Guid. Control Dyn. 11 (3) (1988) 262–270, http://dx.doi.org/10.2514/3.20303.
[17] A. Astolfi, R. Ortega, Immersion and invariance: a new tool for stabilization and adaptive control of nonlinear systems, IEEE Trans. Automat. Control 48 (4) (2003) 590–606, http://dx.doi.org/10.1109/TAC.2003.809820.
[18] J. Davila, L. Fridman, A. Levant, Second-order sliding-mode observer for mechanical systems, IEEE Trans. Automat. Control 50 (11) (2005) 1785–1789, http://dx.doi.org/10.1109/TAC.2005.858636.
[19] D. Lee, K.D. Kumar, M. Sinha, Fault detection and recovery of spacecraft formation flying using nonlinear observer and reconfigurable controller, Acta Astronaut. 97 (2014) 58–72, http://dx.doi.org/10.1016/j.actaastro.2013.12.002.
[20] H.K. Khalil, J. Grizzle, Nonlinear Systems, Vol. 3, Prentice hall New Jersey, 1996.
[21] A. Levant, Higher-order sliding modes, differentiation and output-feedback control, Internat. J. Control 76 (9–10) (2003) 924–941, http://dx.doi.org/10.1080/0020717031000099029.
[22] T. Patel, Satellite Attitude Control Using Environmental Forces Based on Variable Structure Control (Master's thesis), Ryerson University, 2008.